Modeling and Measuring the Bearing Capacitance of Radially Loaded Bearings

Stefan Quabeck, Daniel C. Rodriguez and Rik W. De Doncker
Institute for Power Electronics and Electrical Drives, RWTH Aachen University
Jaegerstraße 17-19
Aachen, Germany
Phone: +49 (0) 241-80 96920
Fax: +49 (0) 241-80 92203
Email: post@isea.rwth-aachen.de
URL: http://www.isea.rwth-aachen.de

Keywords

≪Bearing currents≫, ≪Parasitic elements≫, ≪Impedance measurements≫, ≪Reliability≫

Abstract

Bearing currents can severely reduce the lifetime of electrical machines. The parasitic bearing capacitance causing these currents depends on speed, lubricant temperature, and bearing load. In radially loaded bearings, the capacitance of each bearing ball varies over its angular position, exhibiting high capacitance in the load zone and lower capacitance outside of it. This work proposes a method for measuring the bearing capacitance over the angular position and provides a model that incorporates this effect.

Introduction

Bearing faults are one of the most prevalent fault types in electrical machines [1]. They can be caused by bearing currents that damage bearing balls and raceways, and thus reduce bearing lifetime [2], [3]. Modeling and understanding the electrical behavior of rolling element bearings is essential for improving their lifetime and reducing current in the bearings.

Many publications investigate the electrical behavior of bearings. In [4], the author presents a high-frequency model of an electrical machine that includes the bearing as a lumped model. Lumped models are also used in many other publications as they provide reasonable accuracy at low computational cost, allowing to predict bearing currents [5] or to test bearing current countermeasures quickly in a simulation environment [6]. A method for measuring the parasitic capacitance of a bearing at varying speeds and loads is given in [7]. The authors apply a rectangular voltage waveform to the bearing via a resistor and use the rise time of the bearing voltage to calculate the bearing capacitance. The same measurement method is used in [8] to estimate the bearing capacitance in order to design a capacitive shunt with lower impedance, which guides most of the current around the bearing. The influence of vibrations on the bearing capacitance is investigated in [9].

Many publications estimate the bearing capacitance by means of the Hertzian contact area and other parallel parasitic capacitances. In those publications, the bearing is modeled as one lumped, time-invariant capacitance. This work investigates the parasitic capacitance of a single bearing ball in more detail. The influence of a varying radial load depending on the angular position of the bearing ball is measured. It is shown that the sum of the parasitic bearing capacitances is not as constant over one rotation as other publications suggest.

Fundamentals

In this section, the theoretical background required for modeling the electrical behavior of the bearing is illustrated.

Bearing Capacitance

The parasitic capacitance of rolling element bearings consists of three parts: the capacitance between the inner raceway and outer raceway of the bearing, the capacitance between the inner raceway and the bearing balls, and the capacitance between the outer raceway and the bearing balls. The capacitance between the inner and outer raceways of the bearing is determined by the average dielectric properties of the materials between the races, i.e. the amount of air, lubricant, and steel. This parasitic capacitance C_{IO} can be approximated as a cylinder capacitor with a length W, an inner diameter d_{I}, and an outer diameter d_{O} as

$$C_{\mathrm{IO}} = \frac{2\pi\varepsilon W}{\ln \frac{d_{\mathrm{I}}}{d_{\mathrm{O}}}}. \tag{1}$$

Depending on the amount of lubricant in the bearing and its dielectric properties, ϵ can strongly vary. The capacitances between the bearing balls and the inner and outer raceways mostly depend on the oil film thickness, the dielectric properties of the lubricant, and the Hertzian contact area. The oil film thickness h can be calculated as presented in [10] as

$$h = 2.69 \cdot (\alpha E)^{0.49} \cdot U^{0.68} \cdot W^{-0.067} \cdot (1 - 0.61 e^{-0.73\chi}), \tag{2}$$

where W is the dimensionless load, U is the dimensionless velocity, E is the equivalent modulus of elasticity and $\alpha = 2.3 \cdot 10^{-8} m^2/\mathrm{N}$. Fig. 2b illustrates the film thickness for different lubricant temperatures and rotational speeds assuming a constant load. When the film thickness is low, i.e. for low rotational speeds and high temperatures, the parasitic capacitance is high but the breakdown voltage is low, leading to a high number of breakdowns. When the film thickness increases, the capacitance decreases but the breakdown voltage increases, reducing the number of breakdowns.

In radially loaded bearings, the load is distributed non-uniformly between the bearing balls. We assume that the main load on the bearings is the gravitional force acting on the rotor. Thus, the point with the highest load is expected to be at the bottom of the bearing. The rolling velocity of a bearing ball also changes depending on its angular position. In the load zone, the load gradually becomes higher and the slip of the rolling element decreases. Thus, the oil film is thinnest at an angle of 180° as illustrated in Fig. 6a. Afterward, the load decreases and the slip of the ball increases, increasing the oil film thickness. As the parasitic capacitance of each individual ball is approximately inversely proportional to the oil film thickness, the capacitance reaches its peak value at an angle of 180° as illustrated in Fig. 1. The influence of temperature and speed on the lubricant film thickness in a rolling element bearing is investigated in [5] and [7].

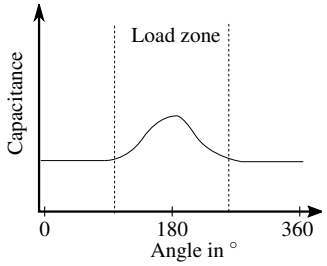

Fig. 1: Expected capacitance

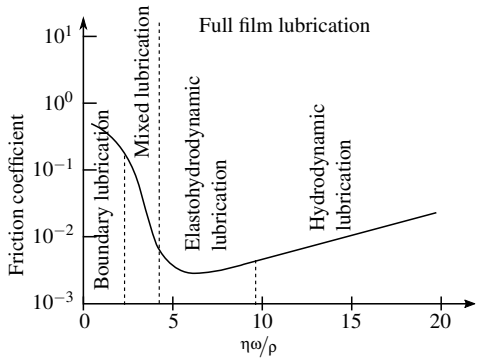

(a) Friction coefficient as a function of the bearing number as per [11]

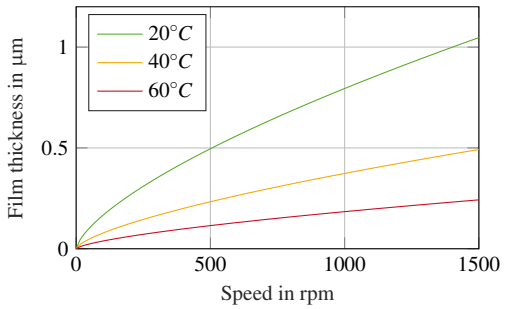

(b) Lubricant film thickness over speed at different temperatures as per [5]

Fig. 2: Bearing properties at different speeds and temperatures

Lubrication Regimes

The oil film thickness strongly depends on the rotational speed of the machine, the contact pressure, i.e., the radial load, and the viscosity of the lubricant, which in turn changes with temperature. Fig. 2a shows the friction coefficient of a rolling element bearing over the bearing number, which consists of the lubricant viscosity η, the speed ω and the contact pressure p. In boundary lubrication, more than 90 % of the radial load rests on surface peaks of the bearing raceways and the balls. At low speeds, low viscosity, i.e., high temperature, and high contact pressure, the electrical behavior of the bearing is therefore assumed to be ohmic. Assuming that the radial load in a typical electrical machine application is constant, with increasing speed, a greater part of the radial load is carried by the lubricant, but there is still direct contact between the raceways and the bearing balls. This lubrication regime is called mixed lubrication. When the bearing is operated in the (elasto)hydrodynamic lubrication regime, i.e., higher speeds and low radial load or low temperature, friction is minimal and there is no direct contact between the raceways and the bearing balls. The electrical behavior is now capacitive and mostly determined by the properties of the lubricant film. Only when the bearing is in (elasto)hydrodynamic lubrication, a constant oil film that can withstand a certain voltage is formed, and therefore, a shaft voltage greater than zero can occur.

Breakdown

There are mainly two events that can lead to a rapid discharge of the bearing capacitance. First, when the bearing leaves hydrodynamic lubrication, due to either a decrease in speed or an increase in radial load or temperature, direct contact between the bearing raceways and balls can occur. The energy stored between the raceways and the bearing balls, i.e., the electrodes of the bearing capacitance, is then discharged through these contact points. Second, when the shaft voltage is higher than the breakdown voltage of the lubricant film, an arc discharge occurs within the bearing. To avoid the first effect, the shaft voltage has to be zero at all times. To avoid the second effect, it is sufficient to keep the shaft voltage below the breakdown voltage. However, the breakdown voltage changes with temperature, speed and radial load. Since the main part of the lifetime of a well-designed bearing is spent in (elasto)hydrodynamic lubrication, electrical discharges are the more relevant breakdown phenomenon.

Model

As already discussed in the previous section, the parasitic capacitance of a rolling element bearing consists of the capacitance between the inner and outer races and the parasitic capacitances between the bearing balls and the bearing raceways. Traditional modeling approaches use a lumped RC-circuit with an additional switch for discharge modeling. In [10], [12], a distributed bearing model is presented. Fig. 3 shows the distributed and lumped equivalent circuit models for a rolling element bearing. Note that two versions of the lumped equivalent circuit are depicted. Fig. 3a is used for most purposes, Fig. 3b

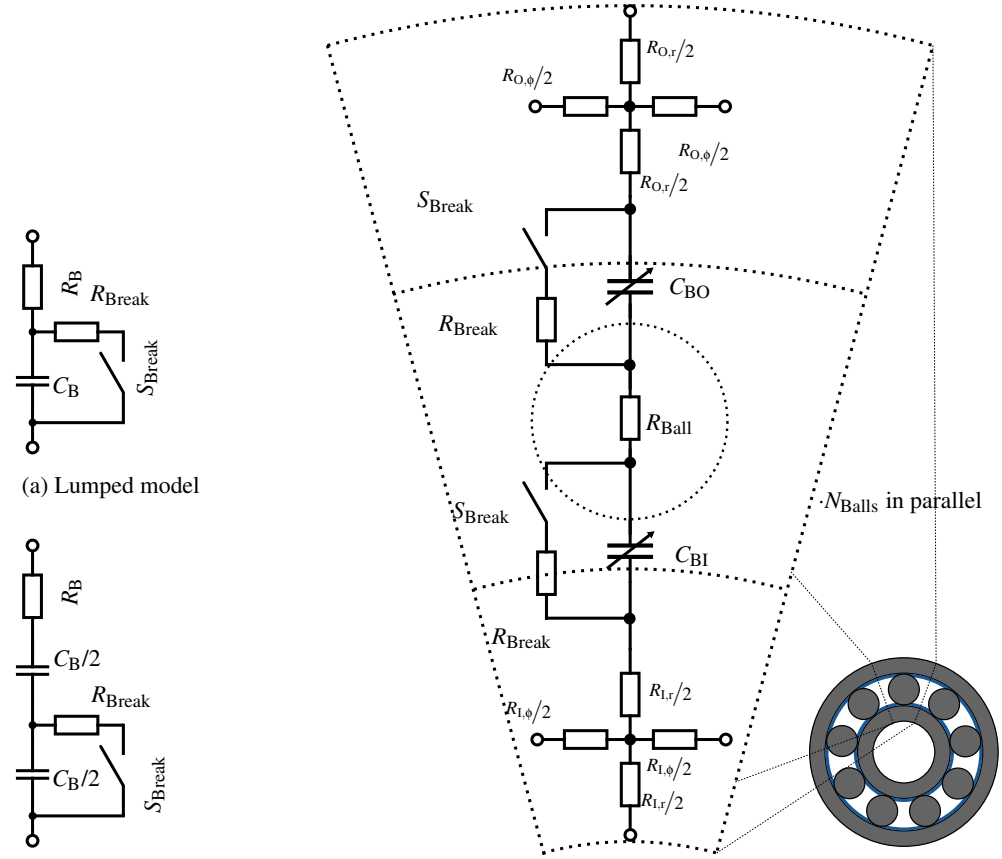

(a) Lumped model

(b) Lumped model with split capacitance

(c) Distributed model

Fig. 3: Lumped and distributed bearing models

is only needed to model partial bearing voltage breakdowns.

While the lumped models exhibit the same electrical behavior from the outside for full breakdowns, and are thus preferable for most modeling purposes, the distributed model shown in Fig. 3c provides further insight into the internal electrical behavior of a rolling element bearing. It allows to individually model the parasitic capacitance of every single bearing ball to the raceways. This enables the discernment of three effects.

First, when a constant voltage is applied to the bearing and the bearing rotates, there will be currents flowing within the bearing, redistributing the charge due to the changes in capacitance. The amplitude of these currents strongly depends on the rotational speed and on the gradient of the parasitic capacitance when a ball enters and exits the load zone.

Second, when a breakdown occurs, the model suggests that the breakdown has two stages. Initially, the parasitic capacitance of the bearing ball where the breakdown occurs is discharged almost immediately as the impedance is low. Then, due to the resulting voltage drop, current from the remaining bearing capacitances, i.e., the parasitic capacitances between the bearing raceways and the parasitic capacitances of the remaining bearing balls, also flows into the breakdown arc until the voltage is low enough and the arc is extinguished. Furthermore, current from outside the bearing can also feed the arc, depending on the source impedance. In an electrical machine, there is only capacitive coupling between the rotor on the inner race and the windings, which act as a source in this case, meaning that the external current flow will decrease quickly.

Third, when only a partial breakdown occurs, which is caused by direct contact between the bearing ball and one of the raceways (e.g., in mixed lubrication or due to irregularities in the raceway surface), the voltage will not be reduced to zero. This effect takes place because only one of the ball-to-raceway capacitances in Fig. 3c is discharged.

Fig. 4 illustrates these effects. Fig. 4a compares the behavior of the lumped and distributed models during a full breakdown. Since the models have been parametrized in a way that their impedances match over a wide frequency range, there is no difference in the breakdown behavior from the outside. However, when looking at the internal charge redistribution currents between the bearing balls in Fig. 5 in the last section of this paper, it can be seen that the internal current amplitudes are much higher than the current seen from the outside of the bearing. This is because most of the energy that is dissipated in a breakdown comes from the parasitic capacitances of the bearing itself and is thus not measurable from the outside.

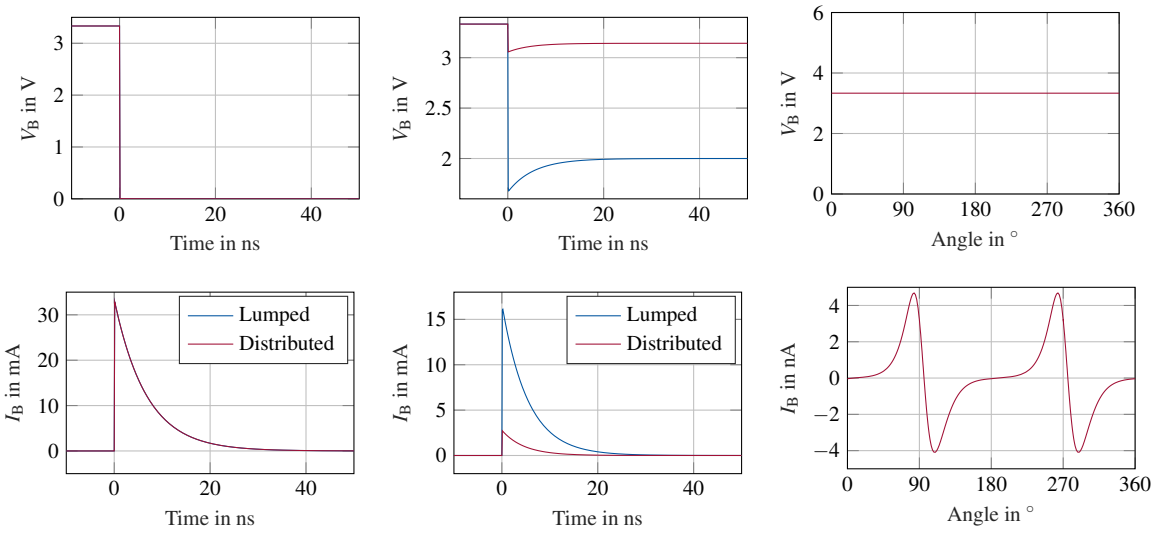

(a) Full Breakdown (b) Partial Breakdown (c) Internal charge redistribution

Fig. 4: Bearing currents and voltages under various breakdown conditions

The partial breakdown phenomenon is illustrated in Fig. 4b. Note that the lumped model has been split into two parts to allow for a fairer comparison, as depicted in Fig. 3b. The voltage drops to approximately 50 % in the lumped model, which was expected from the distribution of the capacitances. In the distributed model, however, the voltage only drops to approximately 93 %. This is because only a small part of the bearing energy is actually discharged, in this case $1/22$ of it. The rest of the energy is redistributed within the bearing. Therefore, the distributed model exhibits a more realistic behavior in case of a partial breakdown.

Finally, Fig. 4c shows the internal charge redistribution within the bearing when no breakdown occurs. A constant voltage of 3.33 V is applied to the bearing. At a speed of 3.000 rpm the current resulting from the change in capacitance amounts to approximately 4.2 nA and can thus be considered irrelevant for the bearing lifetime, especially when compared to the currents occurring during switching events or breakdowns. The unbalanced positive and negative current peaks are due to the calculation method used

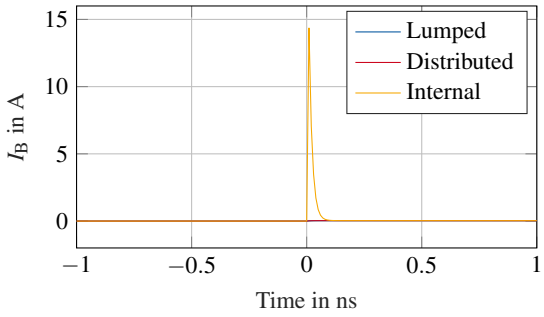

Fig. 5: Breakdown current flowing within the bearing

for the derivation of the bearing capacitance. The charge redistribution current can be calculated as

$$I_\mathrm{B} = V_\mathrm{B}\frac{\mathrm{d}C_\mathrm{B}}{\mathrm{d}t} \rightarrow i_\mathrm{B}(\theta) = V_\mathrm{B}\frac{\mathrm{d}C_\mathrm{B}}{\mathrm{d}\theta}\cdot\omega_\mathrm{Cage}. \tag{3}$$

Even at 16.000 rpm, which is the maximum allowed speed for the bearing under test, the charge redistribution current is expected to be well below the critical thresholds for bearing damage.

Test Bench

In order to confirm the capacitive behavior of a single ball in a ball bearing, which was derived analytically in the previous sections, bearing capacitance measurements are conducted on a radial load test bench.

Radial Load Test Bench

The radial load test bench that is used for these measurements consists of two test bearings and one load bearing in the middle. It is shown in Fig. 6c. The load bearing is connected to a spring to set the radial load. The test bench is driven by an induction machine via a belt drive, which controls the speed of the test bench. Oil is pumped through the bearing in axial direction and heating elements are used to set the temperature and thereby the bearing temperature via a closed-loop control with a temperature sensor at the bearing.

To minimize the effect of additional parasitic capacitances that disturb the measurements, various steps are taken. The load bearing and the rear test bearing are replaced with ceramic bearings. Only the capacitive behavior of the front test bearing is investigated. A specially manufactured 6006 bearing with steel raceways, ten ceramic balls and one steel ball is used as front test bearing. Additionally, the front plate of the test bench, where the front test bearing is mounted, is replaced with polyoxymethylene (POM).

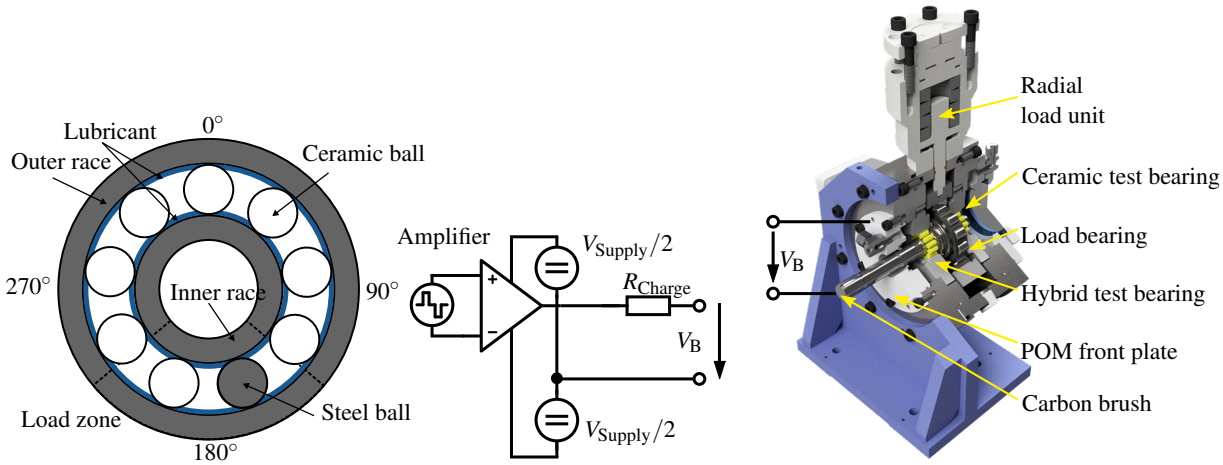

(a) Hybrid Test Bearing with one steel ball

(b) Excitation circuit

(c) Radial load test bench

Fig. 6: Measurement setup

Electrical Excitation

Measuring the bearing capacitance with a reasonable angular resolution at high speeds requires a fast measurement method. Since impedance analyzers or LCR-meters usually have long sweep or settling times, they cannot be used here. Instead, a rectangular voltage waveform is applied to the bearing via a large resistor. The amplitude is set to $\pm 5\,\mathrm{V}$. The excitation circuit is shown in Fig. 6b.

The resistor R_Charge is set to $10\,\mathrm{k\Omega}$ to ensure a charging process that is fast enough to allow the highest required excitation frequency of 20 kHz, but that is still slow enough so that changes in its rise time are

measurable with the temporal resolution of the oscilloscope of 80 MSa/s. All data is directly preprocessed in the oscilloscope and only the rise time, fall time, pulse width, amplitude, and duty cycle of the measured pulse voltage are recorded. The rise and fall times depend on the charging resistance and on the bearing capacitance. Since the charging resistance R_{Charge} is set to a constant value of 10 kΩ, the rise and fall times $\tau_{\mathrm{rise/fall}}$ are directly proportional to the bearing capacitance:

$$C_{\mathrm{B}} = \frac{\tau_{\mathrm{rise/fall}}}{R_{\mathrm{Charge}}}. \tag{4}$$

The circuit is evaluated and calibrated by conducting capacitance measurements on several different capacitors in the range of 10 pF to 1 nF prior to applying it to the bearing and shows good measurement accuracy.

Pulse width, duty cycle, and voltage amplitude are constant during the measurement and are not influenced by the bearing capacitance. However, when a breakdown occurs, these parameters deviate from the set values and thus allow to check the data for validity. If the bearing capacitance is not fully charged before the excitation voltage changes of polarity or if it is discharged prematurely, a breakdown occured and the bearing did not behave purely capacitive in that period. Under these circumstances, the rise and fall times should not be used for capacitance estimation and those specific measurements are thus omitted. In the measurement results, these breakdowns manifest themselves as large capacitance spikes, which often exceed the actual capacitance value by more than 100 %.

Operating Conditions

The bearing capacitance measurements are conducted at a constant radial load of 100 Nm. The bearing capacitance is measured at four different speeds and four different temperatures: 300 rpm, 1.000 rpm, 3.000 rpm and 6.000 rpm and at 20 °C, 30 °C, 50 °C and 80 °C. Automatic transmission fluid is used as lubricant.

Measurement Results

Since the position of the steel ball within the bearing is unknown, the bearing capacitance can only be given over the relative angular position. It can be assumed, however, that the peak of the bearing capacitance corresponds to an angular position of 180° as shown in Fig. 1. The capacitance waveforms are therefore shifted, so that 180° coincides with the peak capacitance, in order to be able to compare them more easily.

Bearing Capacitance

The results of the single steel-ball bearing capacitance measurements are discussed in this section. Fig. 7 shows the measured bearing capacitance over the rotational angle for different speeds and temperatures. Note that the large spikes in the bearing capacitance values indicate breakdowns of the lubricant film where the capacitance could not be measured. At 300 rpm, the bearing capacitance cannot be reasonably extracted from the conducted measurements. Only the capacitance values for 20 °C allow for a rough estimation. The high number of breakdowns suggests either that the bearing is still in mixed lubrication or that the excitation voltage was too high for the still very thin lubricant film.

At 1.000 rpm, the bearing capacitance can be extracted for lower temperatures. The curve at 20 °C indicates a maximum capacitance of 40 pF. At 30 °C the capacitance reaches approximately 50 pF. The increasing number of breakdowns suggests that the excitation voltage should be set to a lower value.

At 3.000 rpm, the capacitance can be extracted for temperatures up to 50 °C, above which the number of breakdowns is too high again. Still, the increase in peak capacitance as temperature increases matches with the expectations from Fig. 2b.

At 6.000 rpm, the capacitance can finally be extracted for all temperatures. Only at 80 °C breakdowns are noticable. The increase of the peak capacitance value with increasing temperature is in accordance with expectations from Fig. 2b.

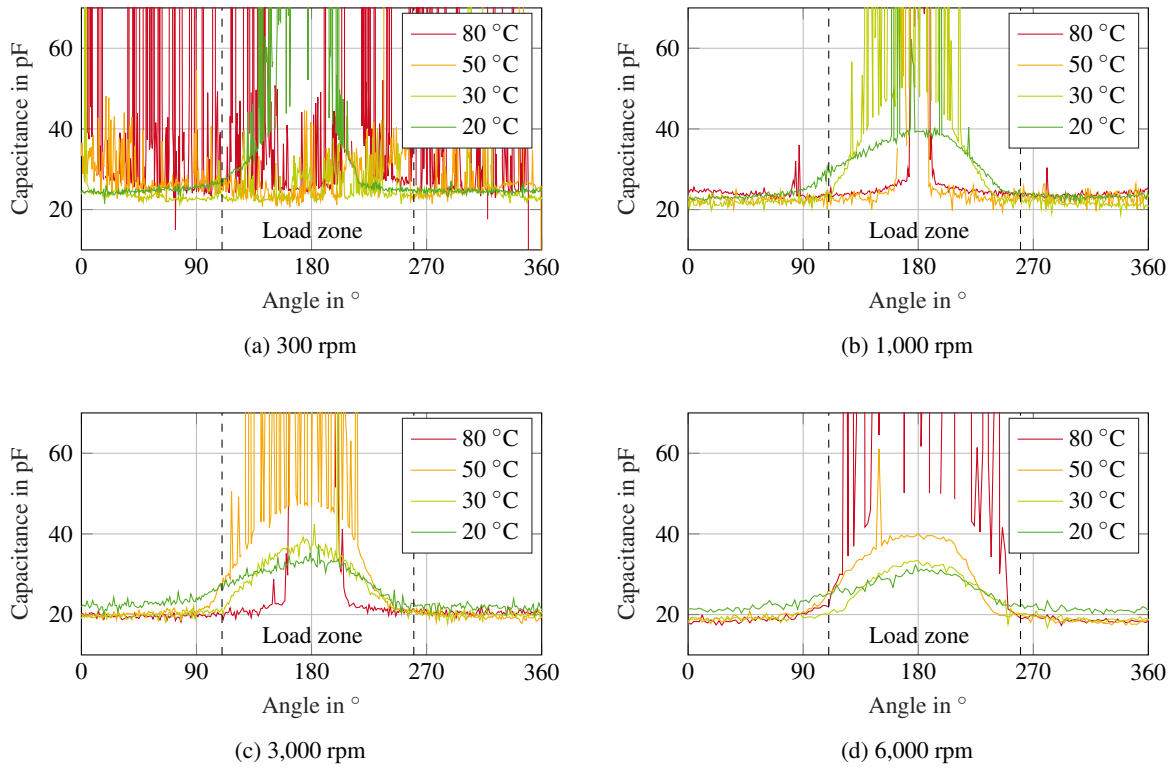

(a) 300 rpm

(b) 1,000 rpm

(c) 3,000 rpm

(d) 6,000 rpm

Fig. 7: Measured parasitic capacitance of a single bearing ball

The capacitance outside the load zone is nearly constant, with only slight deviations over temperature and speed. This indicates that the reduction of viscosity, due to the increase in temperature, and the higher radial forces, due to the increased speed, have nearly no influence on the lubricant film thickness outside the load zone. The capacitance decreases from approximately 25 pF to 20 pF over the whole speed and temperature range. This reduction in capacitance can be attributed to the reduction in raceway-to-raceway capacitance due to the reduced amount of lubricant in the bearing at a higher rotational speed. In addition, at lower temperatures, the higher viscosity of the lubricant leads to higher amounts of lubricant in the bearing and thus increases the raceway-to-raceway capacitance. It was shown that the capacitance peak is strongly influenced by both the rotational speed and the lubricant temperature. The dielectric properties of the lubricant are assumed to be constant over temperature [7].

When overlaying the capacitance measurements with a phase shift of $^{360°}/_{N_{\text{Balls}}}$, a nearly constant capacitance value with a small ripple results, as shown in Fig. 8. However, since this ripple of approximately

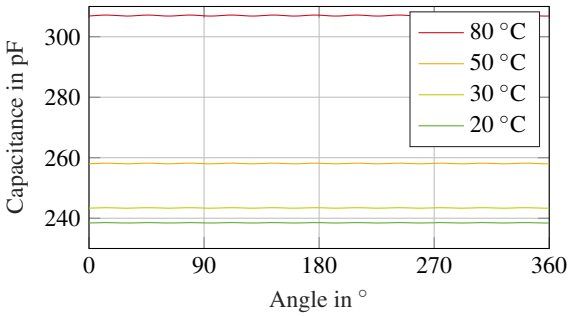

Fig. 8: Parasitic capacitance of the bearing calculated from filtering and overlaying measurements

0.1 pF to 0.3 pF is below 0.1 % of the total bearing capacitance, this is not confirmed with measurements. For further improvement of the measurements, the excitation voltage should be reduced and the measure-

ment frequency should be increased, so that a moving-average filter can be used to reduce the amount of noise on the capacitance measurement.

Conclusions and Outlook

In this work, a distributed parameter model for rolling element bearings has been presented. To confirm the assumption that the parasitic capacitance of individual bearing balls changes over the angular position, a hybrid bearing with one steel ball and ten ceramic balls is investigated. By charging and discharging the bearing with a high-frequency rectangular voltage waveform via a large resistor, the value of the parasitic capacitance is extracted from the rise and fall time. It is shown that at low speeds or high temperatures, the bearing is either in mixed lubrication or the lubricant film is too small to withstand the charging voltage of $\pm 5\,\mathrm{V}$. However, at higher speeds and lower temperatures, bearing capacitance values can be computed. The measurement results show that the parasitic capacitance of an individual ball increases by up to $150\,\%$ when the ball enters the load zone. When overlaying the measured values to model the parasitic capacitance of a full steel bearing, a small capacitance ripple occurs, which was neglected in previous publications.

In future work, the influence of the excitation voltage should be investigated in more detail. With a lower excitation voltage and an increased excitation frequency in combination with additional filters, the capacitance can be determined more precisely and for a wider range of speeds and temperatures.

Additionally, it is shown analytically that due to the changes in capacitance with rotation, even when a constant voltage is applied to the bearing, internal charge rebalancing currents will flow in the bearing. These currents are in the range of $4\,\mathrm{nA}$ for the investigated operating point and are thus assumed as not harmful to the bearing. However, for very high speeds and large bearing capacitances, e.g., in high-speed cylinder bearings, these currents will increase and should be considered in the design phase.

Finally, the model has shown that the internal currents flowing within the bearing during a breakdown are much higher than the current that can be measured from the outside. Precisely modeling the internal currents allows a more accurate estimation of the energy dissipated in the bearing during a breakdown and of the resulting damage. This effect still needs to be confirmed with measurements.

References

[1] J. Kammermann, I. Bolvashenkov, S. Schwimmbeck, and H. Herzog, "Reliability of induction machines - statistics, tendencies, and perspectives," in *2017 IEEE 26th International Symposium on Industrial Electronics (ISIE)*, Jun. 2017, pp. 1843–1847.

[2] M. Kriese, E. Wittek, S. Gattermann, H. Tischmacher, G. Poll, and B. Ponick, "Influence of bearing currents on the bearing lifetime for converter driven machines," in *International Conference on Electrical Machines*, 2012, pp. 1735–1739.

[3] H. Tischmacher and S. Gattermann, "Bearing currents in converter operation," in *The XIX International Conference on Electrical Machines - ICEM*, 2010.

[4] A. Muetze, "Bearing currents in inverter-fed ac-motors," Ph.D. dissertation, Technische Universitaet Darmstadt, 2004.

[5] M. Kriese, E. Wittek, S. Gattermann, H. Tischmacher, G. Poll, and B. Ponick, "Prediction of motor bearing currents for converter operation," in *The XIX International Conference on Electrical Machines - ICEM 2010*, 2010, pp. 1–6.

[6] S. Quabeck, V. Grau, and R. W. De Doncker, "Modeling and mitigation of bearing currents in electrical traction drives," in *2020 23rd International Conference on Electrical Machines and Systems (ICEMS)*, Nov. 2020, pp. 1101–1106.

[7] E. Wittek, M. Kriese, H. Tischmacher, S. Gattermann, B. Ponick, and G. Poll, "Capacitances and lubricant film thicknesses of motor bearings under different operating conditions," in *The XIX International Conference on Electrical Machines - ICEM 2010*, 2010, pp. 1–6.

[8] D. C. Ludois and J. K. Reed, "Brushless mitigation of bearing currents in electric machines via capacitively coupled shunting," *IEEE Transactions on Industry Applications*, vol. 51, no. 5, pp. 3783–3790, 2015.

[9] E. Wittek, M. Kriese, H. Tischmacher, S. Gattermann, B. Ponick, and G. Poll, "Capacitance of bearings for electric motors at variable mechanical loads," in *2012 XXth International Conference on Electrical Machines*, 2012, pp. 1602–1607.

[10] P. Han, G. Heins, D. Patterson, M. Thiele, and D. M. Ionel, "Modeling of bearing voltage in electric machines based on electromagnetic fea and measured bearing capacitance," *IEEE Transactions on Industry Applications*, vol. 57, no. 5, pp. 4765–4775, 2021.

[11] L. Gao, "16 - lubrication modelling of hip joint implants," in *Computational Modelling of Biomechanics and Biotribology in the Musculoskeletal System (Second Edition)*, ser. Woodhead Publishing Series in Biomaterials, Z. Jin, J. Li, and Z. Chen, Eds., Second Edition, Woodhead Publishing, 2021, pp. 415–436.

[12] J. Erdman, R. Kerkman, D. Schlegel, and G. Skibinski, "Effect of pwm inverters on ac motor bearing currents and shaft voltages," *IEEE Transactions on Industry Applications*, vol. 32, no. 2, pp. 250–259, 1996.